C. R. Palevol 16 (2017) 572–584

Contents lists available at ScienceDirect

Comptes Rendus Palevol

www.sciencedirect.com

Human Palaeontology and Prehistory

Was *Australopithecus afarensis* able to make the Lomekwian stone tools? Towards a realistic biomechanical simulation of hand force capability in fossil hominins and new insights on the role of the fifth digit

Australopithecus afarensis *était-il capable de fabriquer les outils du Lomekwien ? Développement d'une simulation biomécanique des capacités de force de préhension d'hominines fossiles et nouvelles perspectives sur l'implication du cinquième doigt*

Mathieu Domalain [a,*], Anne Bertin [b], Guillaume Daver [b,*]

[a] *Département "Génie mécanique et systèmes complexes", institut PPrime UPR CNRS 3346, ENSMA – université de Poitiers, Futuroscope Chasseneuil, 11, boulevard Marie-et-Pierre-Curie, 86962 Poitiers, France*
[b] *UMR-CNRS 7262, Institut de paléoprimatologie et de paléontologie humaine : évolution et paléoenvironnements (IPHEP), université de Poitiers, 86073 Poitiers, France*

ARTICLE INFO

Article history:
Received 10 July 2016
Accepted after revision 22 September 2016
Available online 11 November 2016

Handled by Roberto Macchiarelli and Clément Zanolli

Keywords:
Tool making
Forceful hand grips
Pliocene
Fifth ray
Musculoskeletal modelling
Inverse dynamics

ABSTRACT

While no consensus allows explaining how and when human-like traits arose in fossil hominin hands, the recent discoveries of the Lomekwian stone tools (3.3 Ma) support the view that early hominins were able to use forceful grips in order to manipulate large-sized blocks for pounding activities. Then, assessing gripping abilities of contemporaneous hominin, i.e. *Australopithecus afarensis*, is necessary, particularly with regards to its unusual 5th ray morphology that has been deemed crucial to ensure forceful grips. Here, we present a musculoskeletal simulation based on the *A. afarensis* hand morphology that includes an original 5th carpometacarpal joint. Our first results suggest a limited influence of muscle parameters (e.g., PCSA) and support the value of simulations for studying extinct taxa even in absence of soft-tissue data. Given the inability for the pulp of the 5th ray to face the surface of a large-sized object, the *A. afarensis* hand would have had limited possibility to exert sufficient force to make the Lomekwian stone tools.

Mots clés :
Fabrication d'outils
Force de préhension manuelle
Pliocène
Cinquième rayon

RÉSUMÉ

Alors qu'aucun consensus ne permet d'établir comment ou quand les caractères morphologiques de la main humaine ont émergé au sein du registre fossile, les récentes découvertes des outils de Lomekwi 3 (3,3 Ma) suggèrent que des hominines anciens étaient capables d'utiliser des prises manuelles puissantes pour tailler et manipuler des blocs

* Corresponding authors.
E-mail addresses: mathieu.domalain@univ-poitiers.fr (M. Domalain), guillaume.daver@univ-poitiers.fr (G. Daver).

http://dx.doi.org/10.1016/j.crpv.2016.09.003

Modélisation musculo-squelettique
Dynamique inverse

de grande taille. Afin d'évaluer les aptitudes préhensiles d'un hominine contemporain, une modélisation musculo-squelettique de la main d'*Australopithecus afarensis* a été développée. Une étude de sensibilité a montré la faible influence des paramètres musculaires (e.g., PCSA) nécessairement extraits d'espèces analogues actuelles au regard des paramètres cinématiques de l'articulation carpo-métacarpienne 5 et démontrent ainsi la pertinence de cette approche pour l'étude des taxons fossiles. Nos résultats suggèrent également une capacité limitée de la main d'*A. afarensis* à mettre en contact la pulpe du 5e rayon et la surface d'un objet volumineux. Ainsi, *A. afarensis* aurait disposé d'aptitudes limitées à produire des forces suffisantes pour la manufacture des outils en pierre du Lomekwien.

1. Introduction

Two hypotheses currently provide a theoretical frame for interpreting the acquisition of human-like traits in fossil hominins. One hypothesis states that human-like hand traits arose in early hominins around 2-3 Ma because of intensive manipulative behaviours (including tool use and/or non-lithic tool making) that exceeded those reported among extant non-human primates (e.g., Kivell et al., 2011; Marzke, 1983; Ricklan, 1987; Rolian and Gordon, 2013; Skinner et al., 2015; Susman, 1998). A second hypothesis supports that human-like hand traits evolved due to the adoption of terrestrial bipedalism and the abandonment of arboreal behaviours well before 2-3 Ma (e.g., Alba et al., 2003; Drapeau et al., 2005; Latimer, 1991; Ward et al., 2012), probably around 6 Ma (Almécija and Alba, 2014; Almécija et al., 2010, 2015). This link between bipedalism and human-like hand functions is also supported by the possibility that hands and feet coevolved due to underlying developmental linkages (Rolian et al., 2010).

The recent discoveries of the oldest stone tools dated to 3.3 Ma from Lomekwi 3, Kenya (Harmand et al., 2015), and the putative 3.39 Ma cut-marked bones from Dikika, Ethiopia (McPherron et al., 2010; Thompson et al., 2015; *contra* Domínguez-Rodrigo et al., 2010), allow testing those hypotheses in supporting that early hominins were able to make and use stone tools around 500,000 years before the first occurrences of the genus *Homo* (Villmoare et al., 2015). Also, the lithic reduction techniques inferred from Lomekwian tool replication experiments (among which, the passive hammer technique) suggest that forceful grips at both hands, rather than enhanced hand dexterity, was a major prerequisite for knapping cores as heavy as around 3.4kg (Harmand et al., 2015, extended data, fig. 6). In particular, Harmand et al. (2015: 313) conclude that "The arm and hand motions entailed in the two main modes of knapping [...] suggested for the LOM3 assemblage, are arguably more similar to those involved in the hammer-on-anvil technique chimpanzees and other primates use when engaged in nut cracking than to the direct freehand percussion evident in Oldowan assemblages."

During nut-cracking, chimpanzees use hammerstones heavier than 300 g, with hand grips that involve all digits in more than 80% of the cases (Boesch and Boesch, 1993). They cup large objects of various shapes in a downturned palm, propped by flexed fingers and by the opposed thumb, a type of hand grips that Marzke and Wullstein (1996) define as "cup hold grips". The effectiveness of hand grips postures for the maintenance of a stone tool mainly depends on the forces provided by the hand muscles, the length of the digits, and the ability to "cup" the palm of the hands, so that the hand morphology accommodates to the shape of the object (Marzke, 2013; Marzke and Shackley, 1986; Rolian et al., 2011).

Because the only hominin found in the same geographical and chronological context of the Dikika and Lomekwi findings and whose hand morphology is known is *Australopithecus afarensis*, then assessing its gripping abilities is crucial for answering two questions:

- was *A. afarensis* able to produce muscle forces to incur large-sized stone tools production?
- how could muscle force patterns have looked like in terms of magnitudes and distribution?

1.1. What we know about the functional morphology of the A. afarensis hand: the case of the 5th ray

To date, the *A. afarensis* hand has been described as being human-like due to axial asymmetry of the metacarpal bones and the derived morphology of the distal pollical phalanx, ape-like with regards to its flexor apparatus and mostly intermediate, or unique, when its radial intercarpal and carpometacarpal complexes are considered (Alba et al., 2003; Almécija et al., 2010, 2015; Drapeau, 2015; Drapeau et al., 2005; Kivell et al., 2011; Marzke, 1983; Rolian and Gordon, 2013; Susman, 1998; Tocheri et al., 2003; Ward et al., 2012). Due to this mosaic of traits, it seems then too difficult to interpret individually all morphological traits in order to draw global functional conclusions about the hand of *A. afarensis*. Among the numerous traits described above, the thumb has been the most debated, but traits related to the 5th ray are also crucial to assess functions of the *A. afarensis* hand in the frame of forceful precision grips (e.g., cradle-grip, thumb-to-finger grip) and power grips (Marzke and Shackley, 1986). Marzke and Shackley (1986) and, more recently, Marzke (2013) emphasize that the 5th ray plays a critical role in stabilizing cores with grips by the thumb and four digital pads during hard hammer percussion manufacture of stone tools. Apart from the overall morphology of the 5th ray (i.e. low degree of longitudinal curvature and proper segment proportions), the shape of the hamate-metacarpal V joint (CMC-V) is unique in modern humans, as its mobility allows the 5th ray to

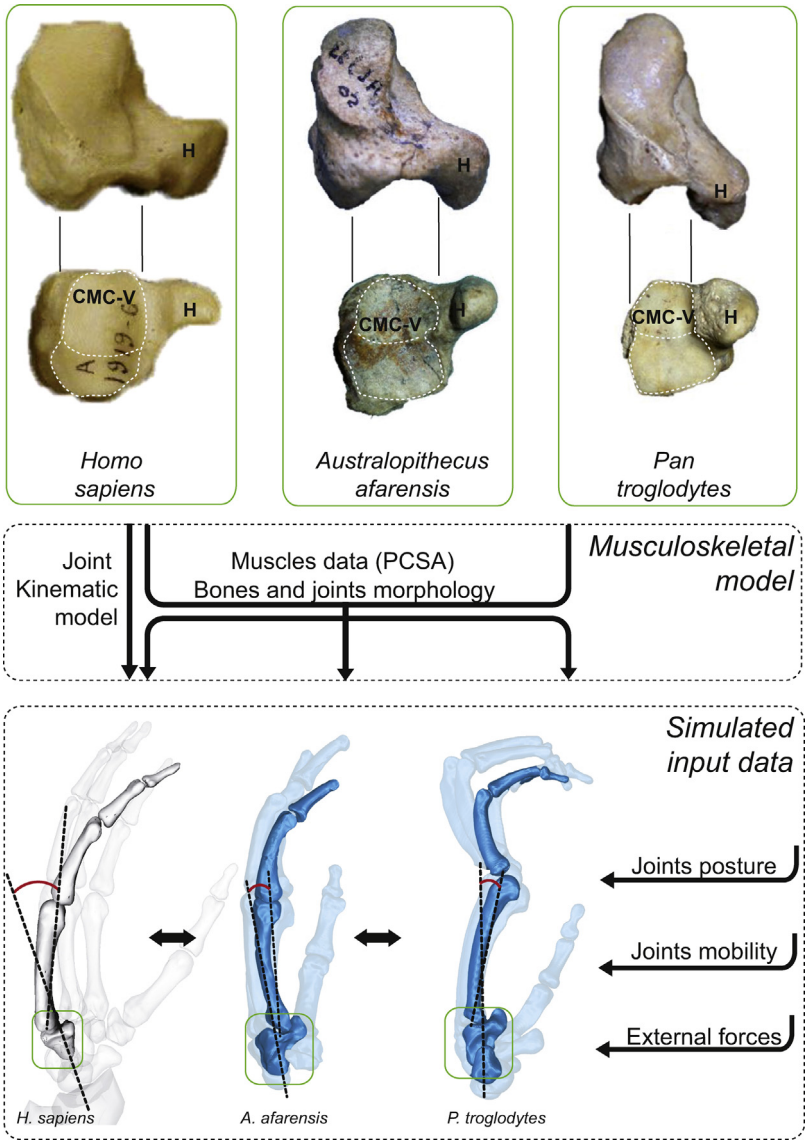

Fig. 1. Research flow chart: green top boxes illustrate the varying shapes of the 5th carpometacarpal joint (CMC-V) and hamulus of the hamate (H) in ulnar (top) and distal (bottom) views in *H. sapiens*, *A. afarensis*, *P. troglodytes*. Inferred ranges of motion at the CMC-V joint are illustrated by red arcs in the bottom box. In the frame of the musculoskeletal model (middle box), sensitivity tests were carried out in order to identify which anatomical parameters are the most influential (i.e. Joint kinematic models of the CMC-V for humans, PCSA and bone dimensions/proportions for the three hominids). After this preliminary analysis, functional impacts of simulated input data (bottom box) on the 5th ray were explored. Skeletal elements are represented at the same size for facilitating comparisons. Hand postures are arbitrary and do not reflect the tested conditions.

Fig. 1. Approche globale et organigramme adoptés pour la présente étude : les encadrés verts du haut montrent les diverses conformations de la 5e articulation carpo-métacarpienne (CMC-V) et de l'hamulus de l'hamatum (H) en vues ulnaire (en haut) et distale (en bas) chez *H. sapiens*, *A. afarensis*, *P. troglodytes*. Chacune de leurs amplitudes relatives de mouvement est illustrée par des arcs de cercle rouges dans les encadrés du bas. Dans le cadre du modèle musculosquelettique (encadré du milieu), des tests de sensibilité ont été menés afin d'établir quels sont les paramètres anatomiques possédant le plus d'influence (modèles cinématiques de la CMC-V pour les humains, PCSA et dimensions/proportions des structures osseuses pour les trois hominidés). À l'issue de cette analyse préliminaire, les impacts fonctionnels des données d'entrée simulées (encadré du bas) ont été explorés. Les éléments squelettiques sont représentés ici à la même échelle pour faciliter les comparaisons. De même, les postures manuelles sont purement illustratives et ne reflètent pas les conditions testées.

oppose to the thumb and exert a better oriented pulp-to-pulp 5th grip force that substantially improves firm maintenance of the hammerstone (Marzke, 1983, 1997, 2013). In comparison, the *A. afarensis* CMC-V morphology has been described as chimpanzee-like (Fig. 1) and is thought to have hampered supination and flexion of the 5th ray (Marzke, 1983, 1997, 2013), so that maintenance ability of hammerstone during tool manufactures was largely limited, if possible (Marzke and Shackley, 1986; Marzke et al., 1992, 1998). Therefore, the assessment of CMC-V mobility and associated force production at the overall 5th ray is fundamental for the better understanding of *A. afarensis* capabilities as no extant analogues to its hand morphology can be easily defined.

1.2. Biomechanical simulations-based approaches and three-dimensional musculoskeletal model of the hominin hand

Functional approaches classically used in palaeontology may be limited for investigating the form-function relationships in complex osteomuscular systems. Experimental biomechanics that involve human experimenters have recently been used to investigate the upper-limb kinematics and grip strength requirements associated with stone tool production and use (Key and Dunmore, 2015; Rolian et al., 2011; Williams et al., 2010, 2012, 2014). However, such approaches, although of interest, are limited in proposing indirect inferences on fossil morphology, whereas the functional impact of morphologies with no extant analogues can be directly and quantitatively estimated with musculoskeletal modelling simulations. This methodological tool is used in the clinical field to test "what-if" scenarios for tendon transfer surgeries (Holzbaur et al., 2005), as well as in ergonomics to study the influence of an object shape on the risk of muscle fatigue or repetitive strain injuries (Vigouroux et al., 2011), to name but a few examples.

In the paleontological field, musculoskeletal simulation has allowed proposing functional inferences in terms of locomotion and bipedalism, even if very partial skeletons are available (Hutchinson, 2004; Nagano et al., 2005; Nicolas et al., 2009; Wang et al., 2004). By contrast, no investigation on hominin hand functions has been carried out to date. In this context, the main advantage of 3D musculoskeletal simulation consists in its capacity of testing hypotheses on organization and shape of unpreserved soft-tissues (mainly muscles and ligaments) from fossil taxa in order to quantify the muscle forces needed for exerting an external force and ensuring joint stability during specific actions.

However, even in well-studied extant taxa such as *H. sapiens*, the obtaining of a realistic musculoskeletal model remains a scientific challenge (Hicks et al., 2015). This is due to the high level of complexity associated with the multi-scale approach necessary to account for a tremendous number of parameters, such as: external interaction with the environment, joint kinematics in relation with bone geometry (Valero-Cuevas et al., 2003), ligament constitutive equations, muscle moment potential on each degree of freedom (DoF) (Lee et al., 2015), muscle contraction dynamics (Romero and Alonso, 2016), etc. As a result, numerous assumptions are generally made and the small mobility of intercarpal and carpometacarpal joints (excepted for the thumb CMC-I) is always neglected in current musculoskeletal models of the hand (Goislard de Monsabert et al., 2014; Lee et al., 2015; Rossi et al., 2015; Sancho-Bru et al., 2003). This limitation needs to be overcome in order to address the role of the CMC-V joint in the production of a forceful finger and palm grips, such as cradle grip (Marzke and Shackley, 1986).

Modelling of extinct species also faces up to the absence of soft tissues quantitative data, such as their moment potential calculated as the product of the physiological cross-sectional area (PCSA, combination of muscle fibre length, pennation angle, etc.) and muscle moment arm. Therefore, before being able to draw trustful conclusions on the capabilities of *A. afarensis* hand, the sensitivity of simulation outcomes to model parameters (bone dimensions, muscle paths and PCSA), as well as input data (external force and joints posture), need to be evaluated.

This contribution has two aims:

- to develop, present and evaluate a simulation framework that includes a musculoskeletal model of *A. afarensis* hand. This model is established and evaluated in comparison to a *H. sapiens* and a *P. troglodytes* model;
- to propose new insights on the putative role the 5th ray may have played in the development of Lomekwian tools production capabilities.

2. Material and methods

2.1. Musculoskeletal model

Opensim 3.3 software (Delp et al., 2007) was used to develop hand models versions for the three taxa: *H. sapiens*, *P. troglodytes* and *A. afarensis*. Opensim is an open-source software platform especially suited for developing models of musculoskeletal structures and creating dynamic simulations of movement. All models were adapted from an original model available on the Opensim repository (https://simtk.org/projects/hand_muscle) based on Lee et al. (2015). The initial model gathers works from numerous studies from the anatomic, biomechanical and physiological fields including those from An et al. (1979). Several levels of modelling are considered. The reference to the kinematic model specifically refers to the mechanical interpretation of the DoF of a joint (e.g., a cardan joint with two intersecting and orthogonal axes of rotation). The constitutive parameters of the anatomical model (sometimes named "anthropometric model" by other authors) include joints parameters (number and range of motion of the DoFs, location and orientation of the rotation axes), bones geometry (length, breadth, height), and musculotendinous attachment sites. The addition of muscles parameters (in particular PCSA) leads to the constitution of the so-called musculoskeletal model. Only modified parameters, as well as details of the 5th ray deemed critical for the simulation output are reported here.

2.2. Bones

Bones specific to the 5th ray are: hamate (Ham), metacarpal 5 (MC-V), proximal phalanx 5 (PP-V), medial phalanx 5 (IP-V), distal phalanx 5 (DP-V). Bone geometry (length, breadth, and height), mass and inertia of *H. sapiens* are taken from the original model and correspond to an average size defined as the 50th percentile of each measurement. Bone geometry of *P. troglodytes* is derived from published dimensions (Drapeau and Ward, 2007; McFadden and Bracht, 2005). Mass and inertia are assumed similar to *H. sapiens*, given that their influence is negligible with regard to the small values compared to the external forces and the static nature of the simulation (Isler, 2006).

The *A. afarensis* bone geometry is based on fossils that were discovered on the A.L. 333 locality of the Hadar

formation, in Ethiopia. All specimens date to c. 3.2 Ma and were scattered on a restricted area of few square meters (Johanson et al., 1982). They share an exceptionally good state of preservation. For the present study, we selected bones based on Alba et al. (2003)'s hypothesis of ray bones re-association of the left *A. afarensis* hand. In order to document musculotendinous attachments sites of the 5th digit muscles, the *Australopithecus* anatomical model was implemented with bone geometries of the right hamate (A.L. 333-50) and the left 5th metacarpal V (A.L. 333w-89) from the same site. Bone geometry was derived from published dimensions (Alba et al., 2003; Bush, 1982; Marzke, 1983; Stern and Susman, 1983), enhanced with author personal observations and measurements of the original fossils and 3D reconstructions (laser scans, NextEngine). Given that all bones cannot be attributed to the same individual, bone dimensions were scaled and symmetrised (for the right hamate) in order to obtain consistent bone dimensions for the 5th ray.

2.3. Kinematic model of the joints

No change was made to the interphalangeal and metacarpophalangeal joints kinematic models and they have been kept identical to the original human hand model (Lee et al., 2015) for the three taxa. Interphalangeal joints (distal DIP-V - and proximal PIP-V) are modelled as hinge joints (one DoF for flexion-extension), and the metacarpophalangeal joint (MCP-V) as a cardan joint (two DoF: flexion-extension and adduction-abduction). Location and orientation of the axes were defined following An et al. (1979), with flexion-extension rotation axes oriented perpendicularly to the parasagittal plan of the bones. Similarly, ab-adduction rotation axis of the MCP-V is perpendicular to the frontal plan. The wrist joint is modelled as a cardan: one DoF in flexion-extension and a second DoF in radio-ulnar deviation.

2.4. Peculiarity of the CMC-V joint

Intercarpal joints were originally modelled as welded joints (0 DoF; in Lee et al., 2015). In this study, *H. sapiens* CMC-V kinematic model is transformed in order to better represent the natural mobility previously reported in anatomical studies (Batmanabane and Malathi, 1985; Dubosset, 1981; El-Shennawy, 2001). Given the limited literature and absence of existing model, two versions of CMC-V are tested in order to add mobility (Fig. 1): 3-DoF, a ball-and-socket/gimbal joint (three independent axes intersecting and orthogonal to each other), and 2-DoF, a saddle joint whose axes are not orthogonal and not intersecting, as it has been suggested for the CMC-I (trapeziometacarpal) joint (Hollister et al., 1992; Li and Tang, 2007).

3-DoF joint centre is located at the most proximal point of MC-V and rotation axes are perpendicular to the anatomical planes of MC-V. 2-DoF associates an ab-adduction rotation axis to another tilted rotation axis that couples flexion-extension and pronation-supination. More precisely, and based on the qualitative description of El-Shennawy (2001), the ab-adduction rotation axis passes through the distal portion of the hamate and is oriented perpendicular to the frontal plan of the palm (approximated as the frontal plan of the third metacarpal). The second rotation axis passes through the proximal end of MC-V, so that the two axes are not intersecting to each other (resulting in an inter-axis distance of 2 mm, and then the absence of unique joint centre). The orientation of the second rotation axis was set to 5° and -12° with respect to the *X* and *Z* axes of the palm of the hand, respectively. The two models (2-DoF and 3-DoF) add potential mobility to the CMC-V joint around its rotation axes and allow the 5th ray to better orient towards the thumb for a pulp-to-pulp pinch (opposition movement), resulting in a more realistic behaviour.

There is no quantitative data published on the mobility of CMC-V for *P. troglodytes*. Based on personal observations and general acceptation in the literature of a restricted mobility (Marzke, 1983; Tuttle, 1969), CMC-V range of motion was considered null in terms of flexion-extension, pronation-supination and abduction-adduction. Similarly, based on the suggestions of Marzke (1983, 2013), *A. afarensis* CMC-V range of motion was assumed to be identical to *P. troglodytes*.

2.5. Muscle data

Twelve muscles whose parameters are primarily based on the original model of Lee et al. (2015) are included in the model: *flexor carpi ulnaris* (FCU), *extensor carpi ulnaris* (ECU), *flexor digitalis superficialis* (FDSL), *flexor digitalis profondus* (FDPL), *flexor digiti minimi brevis* (FDMB), *extensor digiti minimi* (EDM), *extensor digitorum communis* (EDCL), *opponens digiti minimi* (ODM), *abductor digiti minimi* (ADM), 3rd *palmares interossei* (IDP), 4th *dorsales interossei* (ID4), 4th *lumbricales* (L4).

For the *H. sapiens* model, numerical data of muscles attachments sites are based on cadaveric records, experimental studies and imaging techniques (An et al., 1979, 1983). Intermediate via points are included to represent bony contours, as well as muscles volume and large insertion sites (Fig. 2). Muscles insertions and paths remained unchanged from the original *H. sapiens* model (Lee et al., 2015).

P. troglodytes musculoskeletal geometry was adapted from the *H. sapiens* model based on qualitative observations (Diogo, 2013; Diogo et al., 2012). For example, differences include the *flexor digiti minimi brevis* origin on the radial side of *hamulus* (vs. on its convex surface) and the *extensor carpi ulnaris* insertion at the base of PP-V (vs. on MC-V).

Given the absence of soft-tissue data, the *A. afarensis* model was tested with respect to both the *H. sapiens* and *P. troglodytes* musculoskeletal geometry. In the simulations, the only distinctive features accounted for were the dimensions of the bones. Muscle attachment sites are scaled to bone dimensions and plausible associations can be made with specific muscle attachment sites. For example, the long and robust hamulus of *A. afarensis* (Bush, 1982) was interpreted as an origin of the *opponens digiti minimi* located slightly more palmarly compared to *H. sapiens*.

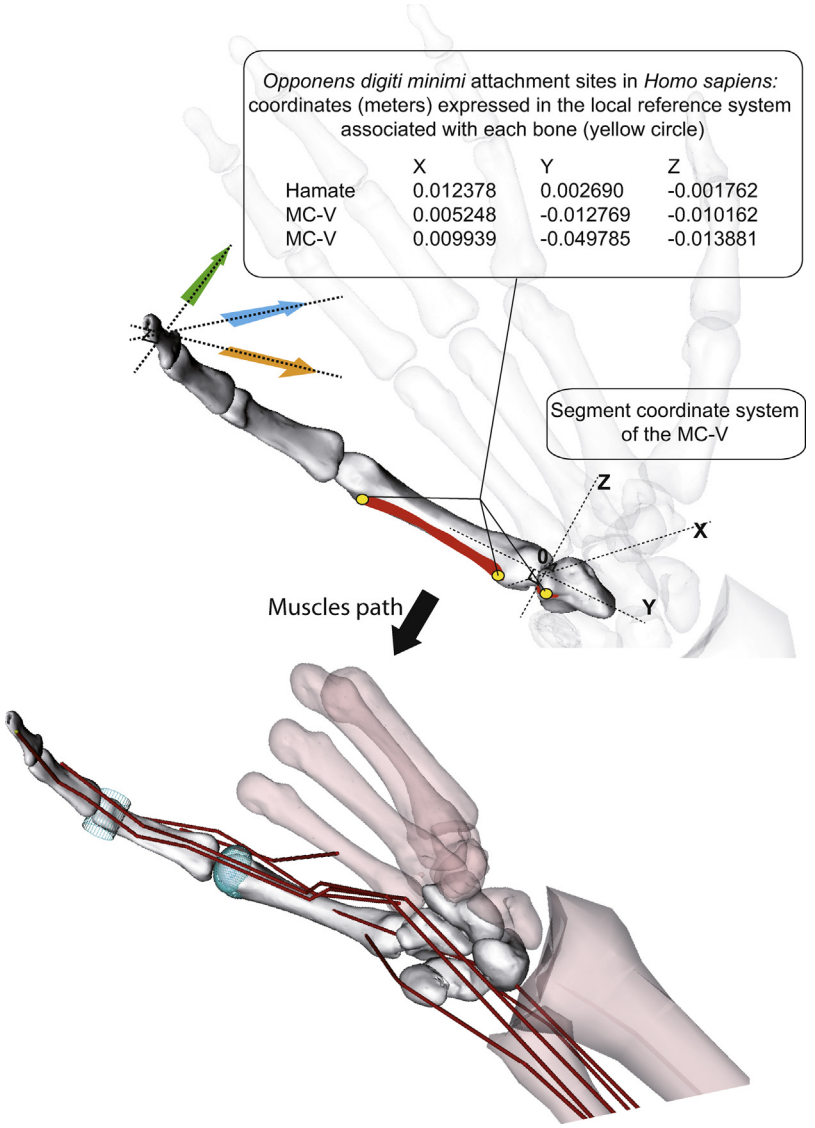

Fig. 2. Bases of the musculo-skeletal model used in the present study. Top: depiction of the 5th ray of the hand showing the segment coordinate system of the MC-V with *X*, *Y*, and *Z* axes oriented palmarly, proximally, and radially. Example of *opponens pollicis brevis* muscle attachment sites as described in the literature (red areas) and modelled (yellow circles). The three orientations of external force simulated at the distal phalanx are represented by the arrows (palmar: orange; radial: green; palmar-radial: blue). Bottom: three-dimensional musculoskeletal model of the 5th ray. The radius, ulna and all metacarpals are represented for illustrative purposes. Muscles of the 5th ray are represented using line segment paths to which origin and insertion points (see above) and via points (represented by breaking lines) were assigned. Wrapping surfaces (blue volumes) were used to conform to moment arms measured experimentally and take into account soft tissues and bone reliefs. Hand postures are arbitrary and do not reflect the tested conditions.
Fig. 2. Fondements du modèle musculo-squelettique utilisé dans cette étude. En haut, représentation du 5e doigt, illustrant le système de coordonnées segmentaires du métacarpe 5 avec les axes *X*, *Y* et *Z* orientés en direction palmaire, proximale et radiale. Les zones d'insertions musculaires sont telles que décrites dans la littérature (zones rouges) et modélisées (cercles jaunes) pour le muscle *opponens pollicis brevis*. Les trois orientations de forces externes simulées à la phalange distale sont indiquées (palmaire : flèche orange ; radiale : flèche verte ; palmaire-radiale : flèche bleue). En bas, modèle musculo-squelettique tridimensionnel du 5e rayon. Le radius, l'ulna et les métacarpiens sont représentés à titre illustratif. Les muscles du 5e rayon sont représentés par un ensemble de lignes segmentées pour lesquelles ont été assignés des points d'origine, d'insertion (cf. figure du haut) et des points de passage (représentés par une ligne brisée). Des surfaces de contournement (volumes bleus) ont été utilisées afin de respecter les bras de levier mesurés expérimentalement et ainsi tenir compte des reliefs osseux et des tissus mous. Les postures manuelles sont représentées de manière arbitraire et ne reflètent en rien les conditions testées.

Muscle properties (muscle mass, fibre length, pennation angle, etc.) and resultant force-length-velocity relationships implemented in the Opensim (Hill-type) muscle model originate from several imaging and experimental studies. Given the limited literature, and even if the influence of muscle properties on model output has been deemed modest (Bolsterlee et al., 2015; Valero Cuevas et al., 2008), three databases of PCSA were investigated (Table 1): PCSA-Homo1, the database used in the original model (Lee et al., 2015) that gathers data from different collections

Table 1
Comparison of the three different physiological cross-sectional area (PCSA) databases: Homo1 (Original model), Homo2 (Chao, 1989) and Pan (Ogihara et al., 2005).
Tableau 1
Comparaison des valeurs de PCSA (section de coupe physiologique) des trois différentes bases de données : Homo1 (modèle original), Homo2 (Chao, 1989) et Pan (Ogihara et al., 2005).

PCSA (cm^2)	FCU	FDMB	ODM	ECU	ADM	EDM	EDCL	IDP	ID4	L4	FDSL	FDPL
Homo1 (Original model)	10	0.4	2.9	3.5	0.9	1.5	0.5	1.3	1.1	0.2	2.1	2.1
Homo2 (Chao, 1989)	3.42	0.54	1.1	2.6	0.89	0.64	0.4	0.61	0.91	0.06	0.4	2.2
Pan (Ogihara et al., 2005)	9.53	1.48	1.6	2.58	1.48	0.69	2.58	1.2	2.3	0	1.54	3.01

(Jacobson et al., 1992; Lieber et al., 1992); PCSA-Homo2, from data published in Chao (1989); and PCSA-Pan, based on *P. troglodytes* data from Ogihara et al. (2005).

2.6. Simulated input data

2.6.1. CMC-V joint mobility

The influence of using one or another kinematic model (0-DoF vs. 2-DoF vs. 3-DoF) for *H. sapiens* CMC-V is analysed prior of investigating the evolutionary hypotheses. In other words, we tested whether CMC-V joint should be supposed equilibrated by passive constraints only (0-DoF), a combination of passive constraints and muscle forces (2-DoF), or muscle forces only (3-DoF).

2.6.2. Joints posture and 5th ray orientation

DIP-V, PIP-V and MCP-V (both flexion and abduction) joint angles were set to 20°, so that the 5th digit was slightly flexed and abducted. The wrist joint was set in neutral position (0° in flexion-extension and 0° in radio-ulnar deviation). Regardless joint mobility, several postures of the CMC-V joint were simulated in order to mimic the diversity of forceful hand grips and represent the different mobility associated with each taxon. Flexion, abduction and supination at CMC-V included three modalities: 0°, 5°, and 10° (10° ≈ maximum joint excursion; Batmanabane and Malathi, 1985; Dubosset, 1981; El-Shennawy, 2001).

2.6.3. External force

In order to maintain a large-sized object, the 5th ray must exert an external force oriented towards it. It is represented by a point contact force applied at the middle length of DP-V. Here, three different force directions (expressed in PP-V referential system; see Fig. 2) – i.e. a palmar force, a radial force, and a combined palmar/radial force – are simulated in order to take into account the different orientation of the distal phalanx, regarding to the object due to the various CMC-V postures. In a first analysis, a one-unit (1 Newton) external force is simulated to compute resulting muscle forces ($n = 12$) and, in a second analysis, the maximal external force the model is capable to exert is calculated.

2.7. Output data and analysis

2.7.1. Computation of muscle forces

Joint stability is ensured by both the passive structures such as joint congruence, ligaments, fasciae, and joint capsules, and the active role of muscles. Muscle forces are computed using an inverse dynamics approach with joint postures and external force magnitude/direction as inputs. Unmodelled DoF are *de facto* assumed welded DoF, so that they are not equilibrated by muscles but by passive constraints (not calculated). Therefore, muscle forces necessary to equilibrate CMC-V joint vary depending on the conditions (0-DoF, 2-DoF and 3-DoF). The wrist was not artificially welded, so that we did not eliminate the need for the muscles of the 5th ray that cross the joint (FCU, ECU, FDSL, FDPL, EDCL) to equilibrate its two DoF. Muscle forces are calculated according Newton–Euler's laws of motion, so that they counteract the external force and equilibrate all non-welded DoF [Eq. (1)], resulting in a stable posture (static condition):

$$\vec{M}_{\vec{F}_{ext}} + \sum \vec{M}_{\vec{F}_{muscle_i}} = \vec{0} \quad (1)$$

with $\vec{M}_{\vec{F}_{ext}}$ the moment of the external force at a joint and $\sum \vec{M}_{\vec{F}_{muscle_i}}$ the sum of moments exerted by all muscle crossing the joint. Muscle moment $\left(\vec{M}_{\vec{F}_{muscle_i}}\right)$ results from the cross-product of muscle force $\left(\vec{F}_{muscle_i}\right)$ and its moment arm $\left(\vec{L}_i\right)$.

The indeterminate problem associated with muscle redundancy is solved with a classical optimisation scheme (Prilutsky and Zatsiorsky, 2002; Vigouroux et al., 2009) that minimises muscle activation square Eq. (2) among the muscles of the 5th ray such as:

$$\min : f(F_i) = \sum_{i=1}^{12} (a_i)^2 \quad (2)$$

2.7.2. Data analysis

Dependant variables analysed are simulations outputs of :

- muscle forces to exert a unit external force ;
- maximal external force a model can exert.

Numerous simulations based on combination of constitutive parameters of the musculoskeletal model (CMC-V

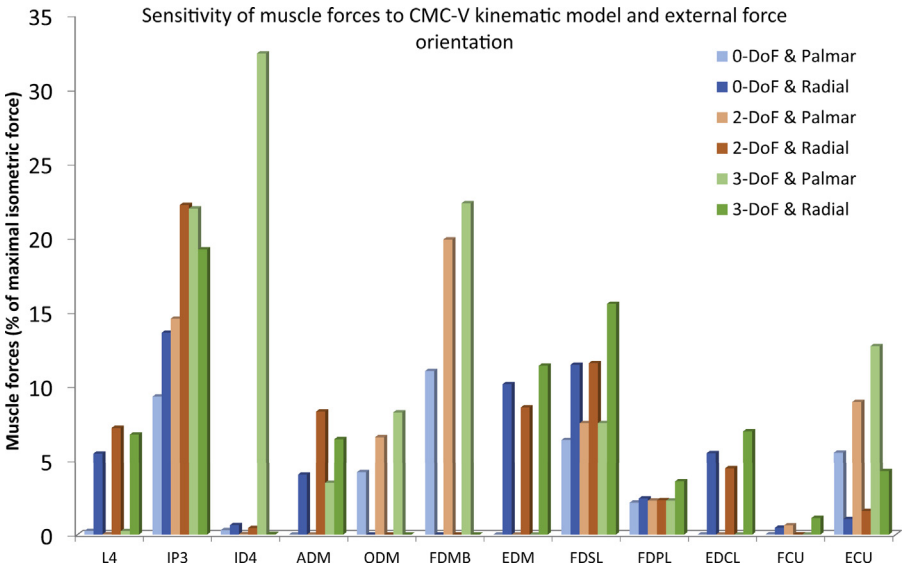

Fig. 3. Muscle forces (expressed as a percentage of their maximal isometric force) to exert a 1-N external force, as a function of CMC-V kinematic model and external force orientation. *H. sapiens* musculoskeletal model.
Fig. 3. Forces musculaires (exprimées en pourcentage de leur force isométrique maximale) pour produire une force externe de 1 N en bout de doigt selon le modèle cinématique de la CMC-V et la direction de la force externe. Modèle musculo-squelettique *H. sapiens*.

kinematic model, anatomical model, PCSA database) and input data parameters (CMC-V joint posture and external force direction) were run. Results are synthesised in terms of sensitivity of simulation outputs and relevance from an evolutionary perspective.

3. Results

3.1. On the choice of a new kinematic model of CMC-V for H. sapiens

Muscles forces necessary to exert a 1-N external force are calculated for the three CMC-V kinematic models (0-DoF vs. 2-DoF vs. 3-DoF). Overall, mean muscle forces are 1.8 ± 2.4 N, 2.8 ± 3.8 N, and 4.4 ± 5.3 N for 0-DoF, 2-DoF, and 3-DoF, respectively. There is a significant effect of the kinematic model on muscle forces ($F[2,11] = 5.27$, $P = 0.013$). More precisely, the 3-DoF leads to significantly higher muscle forces than 0-DoF, while no significant difference was found between 2-DoF and 0-DoF. As an example, Fig. 3 compares muscle forces (as a percentage of their maximal isometric force) for the three kinematic models in two external force directions (palmar-radial direction not represented for clarity). Again, it illustrates that 3-DoF (green bars in Fig. 3) leads to higher muscle forces. It also highlights specific discrepancies, such as for the 4th *dorsales interossei* muscle (ID4) force, which is especially high (~32%) for the 3-DoF + palmar force direction condition.

ID4 is the primary limiting factor in the estimation of maximal external force. The maximal external force the model is able to exert (Table 2) is smaller under the 3-DoF model. The difference is especially high when the force has to be oriented palmarly; in such a case, the external force is 4.2 N, which is 50% less than calculated under the two other conditions.

3.2. Sensitivity to PCSA database

Before running the simulations and calculating muscle forces, muscles PCSA of the three databases (Table 1) were compared. On average, PCSA-Pan are 6% higher than PCSA-Homo2 and 51% than PCSA-Homo1, with notable differences for some muscles such as the FDSL (2.1, 0.4 and 1.54 cm^2 for PCSA-Homo1, PCSA-Homo2 and PCSA-Pan, respectively) and the ID4 (1.1, 0.91 and 2.3 cm^2 for PCSA-Homo1, PCSA-Homo2 and PCSA-Pan, respectively). The root mean square deviation (RMSD) between PCSA-Homo1 and PCSA-Homo2 database is higher (2.07) than between PCSA-Homo1 and PCSA-Pan (0.99) and between PCSA-Homo2 and PCSA-Pan (1.98). As a matter of course,

Table 2
Magnitudes of the maximal external forces possible to exert as a function of CMC-V kinematic model and force direction.
Tableau 2
Intensité des forces externes maximales susceptibles d'être produites selon le modèle cinématique de la CMC-5 et la direction de la force externe.

DoF	Palmar force (N)	Palmar-radial force (N)	Radial force (N)
0-DoF (welded joint)	9	17.8	8.6
2-DoF (coupled)	9.3	18.1	9.8
3-DoF (free joint)	4.2	16.2	7.2

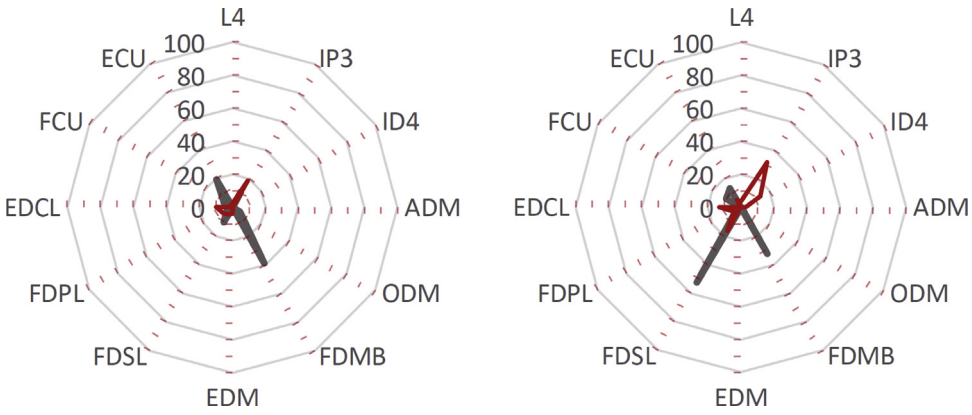

Fig. 4. Radar plot of muscle forces (percentage of their maximal isometric force) to exert a 1-N external force oriented palmarly (grey) and radially (red) for 2 PCSA databases: PCSA-Homo1 (left) and PCSA-Homo2 (right).
Fig. 4. Diagramme des forces musculaires (pourcentage de leur force isométrique maximale) produites pour exercer une force externe de 1 N orientée en direction palmaire (en gris) et radiale (en rouge) pour deux bases de données de PCSA : PCSA-Homo1 (à gauche) et PCSA-Homo2 (à droite).

these discrepancies lead to notable differences in the estimated muscle forces.

Fig. 4 illustrates muscle forces (as a percentage of their maximal isometric force) to exert a 1-N external force for 2 PCSA databases: PCSA-Homo1 (left) and PCSA-Homo2 (right) and 2 external force directions (palmar and radial). A large difference can be observed for the FDSL muscle force (there is also a large difference in the PCSA of FDSL between the two models: 2.1 cm^2 for PCSA-Homo1 vs. 0.4 cm^2 for PCSA-Homo2). In general terms, and beyond specific differences, results gathered from the numerous simulations exhibited a similar muscle forces distribution pattern whatsoever the PCSA database used. The influence was mainly on the amplitude of the maximal external force the model is able to exert: PCSA-Homo1 consistently leads to a smaller maximal force.

3.3. Influence of the anatomical model of A. afarensis

The %RMSD between muscle forces estimated from simulations based on the anatomical model of *H. sapiens* and simulations based on an anatomical model of *P. troglodytes* is 13% (average across force direction; CMC-V posture and PCSA database conditions). Overall, simulations run by using an anatomical model based on *P. troglodytes* demonstrated a higher capacity of external force, but muscle force patterns were rather similar (the greatest differences were observed for ECU and ADM).

3.4. Combined influence of CMC-V joint posture and external force orientation

As illustrated in Fig. 5, there is a notable influence of both CMC-V joint posture and external force direction on muscle forces to exert a 1-N external force. Overall, muscle forces are decreased when CMC-V can flex and supinate (green and yellow bars on the graph), compared to the condition where the joint is in a 0° of flexion, supination and abduction (blue and red bars). This result is exacerbated when the external force is oriented radially (blue vs. red bars and green vs. yellow bars). For example, mean muscle forces (average across all simulations tested) to exert a 1-N force are: 4.1 ± 5.5 N, for CMC-5 0° flexion and palmar force; 2.7 ± 3.8 N, for CMC-5 10° flexion and palmar force; 3.7 ± 3.5 N, for CMC-5 0° flexion and radial force; and 2.5 ± 2.6 N, for CMC-5 10° flexion and radial force. Furthermore, the maximal external force the model is capable to exert tends to be 50% higher (15.5 ± 3.9 N) in conditions associated with a palmar-radial force orientation, than with a radial force orientation (7.7 ± 2.5 N), or a strict palmar force direction (9.8 ± 2.1 N).

4. Discussion

4.1. Limitations

Several limitations other than those already exposed must be acknowledged before going into the interpretation of the results. The external force was assumed here as a single force vector located on DP-V (the distal phalanx), while a more accurate simulation would include multiple interactions that arise at the interface between the digit and a large-sized object (Goislard de Monsabert et al., 2012; Rossi et al., 2015). However, such data are still unavailable for the 5th digit in the frame of Lomekwian tool making replication.

Also, no passive structure was included in the original model. The absence of passive structure contribution in the stability of unwelded DoF is frequent in musculoskeletal modelling, and assumed to be reasonably realistic when joints are positioned at mid-range of joint excursion, which seems reasonable here in the context of a forceful hand grip posture of a tool. Even if difficult to identify, an effort should be made to model passive constraints, especially at the CMC-V joint, whether using an analytical (Majors and Wayne, 2011) or a more global approach (Domalain et al., 2010; Gabra and Li, 2016). Lastly, the constitution of the musculoskeletal model was based on the last published data, such as those from Lee et al. (2015), that beneficiate from both anatomical records of tendon locations and experimentally calculated moment arms. However, all the complexity of the hand

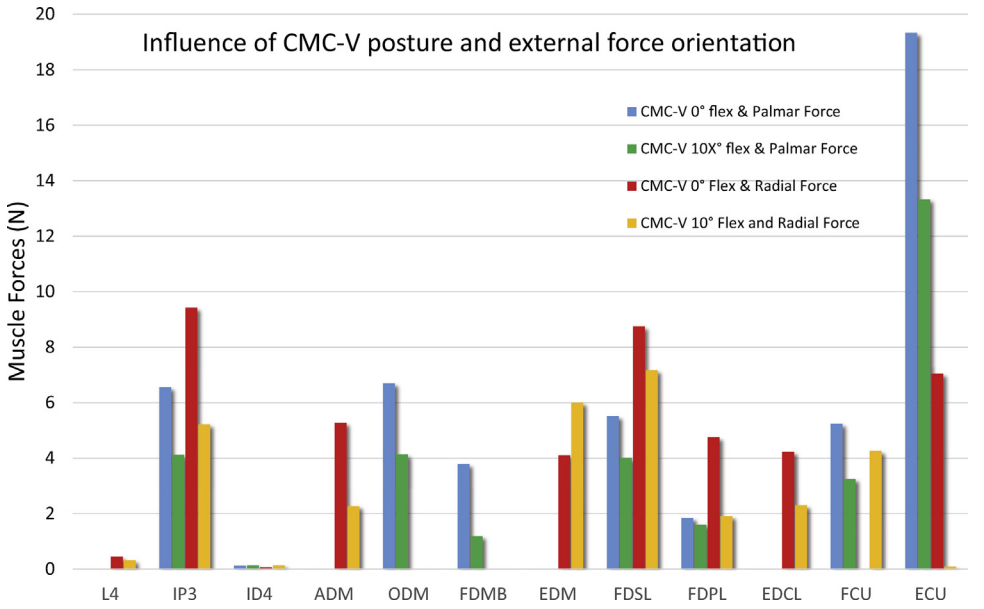

Fig. 5. Muscle forces (N) to exert a 1-N external force (example from *A. afarensis* musculoskeletal model with PCSA-Homo2). Two conditions of CMC-V posture and external force orientation are illustrated.
Fig. 5. Forces musculaires (N) pour exercer une force externe de 1 N (exemple du modèle musculo-squelettique *A. afarensis* comprenant la base de données PCSA-Homo2). Seules deux modalités du modèle cinématique de la CMC-5 et d'orientation de la force externe sont illustrées.

muscular system cannot be perfectly reproduced and the model includes several simplifications whose consequences need to be assessed. For example, the intrinsic muscle connection to the dorsal aponeurosis and FDP tendon could not be modelled. Instead, muscle attachment points were set so that moment arms matched experimentally measured moment arms (Lee et al., 2015). The simplification of the extensor mechanism has also been found to have little influence on flexor forces estimations when the location of external force application is distal to the PIP joint (Li et al., 2001).

4.2. Modelling considerations on the kinematics of the CMC-V joint

The choice of a kinematic model of CMC-V joint was a major modelling issue to obtain simulations that include a more realistic *H. sapiens* 5th ray. The few hand musculoskeletal models that exist consider CMC-V as a fixed/welded joint, so that joint stability is brought by passive structures only. The estimation of muscle forces is thus facilitated, but inexact. Besides, this assumption prevents the 5th ray to adequately orient towards the thumb.

Our results demonstrate that adding mobility using a 3-DoF (gimbal) kinematic model may lead to a 50% decreasing in maximal external/grip force in *H. sapiens* (Table 2). On the contrary, the specific 2-DoF (saddle joint) model we developed does not decrease maximal force capacity and is thus likely to be more realistic, both in terms of mobility and stability. The 2-DoF kinematic model was therefore adopted for the rest of the study for the *H. sapiens* CMC-V joint. This is in line with previous studies on CMC-I (trapeziometacarpal joint) that similarly recommended against assuming a full 3-DoF model (Domalain et al., 2011; Hollister et al., 1992; Valero-Cuevas et al., 2003).

P. troglodytes and *A. afarensis* CMC-V were modelled as a 0-DoF joint. While it may seem arbitrary and a little mobility may exist, the results show a limited difference of external force potential between the 0-DoF and the 2-DoF models. This means that it has little importance whether the *A. afarensis* CMC-V joint is assumed to be equilibrated by passive structures only (0-DoF), or by a combination of passive structures and muscle forces (2-DoF). Ultimately, it is the ability to adequately orient the 5th ray towards the hand-held object that influences the most the potential of maximal external force.

4.3. Sensitivity of the simulation to PCSA

Facing the absence of soft tissue data for extinct species, databases from an extant analogue has to be used (Hutchinson, 2004; Nicolas et al., 2009). In order to ensure that the influence of this parameter on simulation outcomes was limited, we tested three PCSA databases related to *H. sapiens* (PCSA-Homo1 and PCSA-Homo2) and *P. troglodytes* (PCSA-Pan). Surprisingly, intrataxic variations (between the two *H. sapiens* PCSA databases) are larger than intertaxic variations (between the two *H. sapiens* PCSAs and PCSA-Pan). Using PCSA-Pan leads to the highest potential of external grip force but, overall, muscle force patterns remain similar for the three databases.

The difference between the two *H. sapiens* PCSAs highlights the difficulty to accurately estimate this parameter and the need for a unified database, rather than data gathered from different works and specimens. Nevertheless, the RMSD between PCSA conditions remains smaller than between CMC-V kinematic model condition and between

anatomical model conditions. Altogether, these results would suggest a rather limited sensitivity of simulation outputs to muscle parameters (fibre length, pennation angles, etc.) and tend to argue in favour of using simulation approaches to study extinct species even with the unavoidable absence of soft-tissue data.

4.4. On the influence of the anatomical model of *A. afarensis*

Two versions of the *A. afarensis* anatomical model based either on the *H. sapiens* and the *P. troglodytes* anatomical models were compared. For both, a few specific characteristics resulting from the scaling to fossil bone dimensions were introduced, or were postulated from their direct observation (e.g., origin of *opponens digiti minimi* based on specific shape of *A. afarensis* hamulus).

Overall, simulations that were run with an anatomical model based on *P. troglodytes* demonstrated a higher external force capacity than those adopting a *H. sapiens* model. The results also showed that the anatomical model has a greater influence than PCSA on outcomes data. The cross-analysis of all the simulations further suggests that the anatomical parameter leading to the greatest difference in outcomes data is muscle attachment sites. Muscle attachment sites influence muscle moment arm and thus its moment potential (capacity to exert a "rotation force" at a given DoF). Attachment sites are expressed in a bone reference system (see Fig. 2), thus, the consistency between muscle attachment sites and the kinematic model of the joints (rotation axes location/orientation) is as critical as the precision of the joint model itself.

The use of an accurate and consistent database, even if obtained on a single individual (see Mirakhorlo et al., 2016), would likely contribute to more accurate simulations for *H. sapiens*. For extinct taxa, such as *A. afarensis*, a more accurate morphofunctional analysis of the bones (Chaudhari et al., 2014; Daver et al., 2012; Orr et al., 2010) associated with a validation procedure on extant taxa, should also help refining putative muscle attachment sites.

4.5. On the importance of CMC-V orientation in forceful hand grips

The putative low mobility of *A. afarensis* CMC-V joint leads to low flexion, abduction and supination angles that restrict the ability to optimally orient the pulp of the 5th ray towards the hand-held object. Indeed, in the frame of a forceful and cup hold grip, there exists a logical relationship between joint posture and external force orientation, such as the less abducted and pronated the 5th ray, the more radial the direction of the grip force is.

Simulation results (Table 2) show that grip force potential is maximal when oriented in a palmar-radial direction, and decreases by ~50% when directed in a true radial direction. This highlights the importance of being able to adequately orient the pulp of the 5th ray so that a palmar-radial force is applied towards the object. Moreover, whatsoever the direction of the external grip force, results tend to show that, when CMC-V can be flexed (10° in our examples), muscle forces are lower for a given amount of external force (Fig. 5).

Those two phenomena are linked to the complex interaction of muscle moment arms that vary as a function of joint angles and direction of the external force that influences joint moments. Altogether, this suggests that *A. afarensis* inability to ideally orient the 5th ray could have constituted a limiting factor for exerting a grip force strong enough for large-sized stone tool making, which is in line with previous speculations (Marzke, 1983, 2013).

5. Conclusions and perspectives on evolutionary hypotheses

In this study, we present the first musculoskeletal simulation that integrates most aspects of the *A. afarensis* hand morphology, with a special emphasis on its 5th ray. Accordingly, we developed an original model of the 5th carpometacarpal joint that includes coupled degrees of freedom and provides more realistic mobility and stability to the *H. sapiens* joint. Our results suggest a limited influence of muscle parameters (fibre length, pennation angle, etc.) and argue in favour of using simulation approaches to study extinct species, even with the absence of soft-tissue data.

The musculoskeletal modelling of *A. afarensis* hand would still benefit from new refinements, but this study already enables to gain new insights on the putative ability of this taxon to make tools. In particular, those first results suggest that the inability for the pulp of the 5th ray to adequately face the surface of large-sized object would have limited the possibility to exert sufficient force to hold blocks such as the ones manipulated at Lomekwi 3. As a perspective, the biomechanical simulation of the fossil hominin hands would benefit from more realistic input data from *in vivo* tool replication protocols and from a better documentation of the hand of penecontemporaneous species of *A. afarensis*.

Acknowledgements

We dedicate this contribution to the memory of Laurent Puymerail, our friend. We are also indebted to F.K. Jouffroy, who inspired this work and unfortunately recently passed away. We also thank the guest editors, Roberto Macchiarelli and Clement Zanolli, for their invitation for submitting a manuscript to this thematic issue as well as Sonia Harmand, Sandrine Prat and the two reviewers for their valuable comments on a previous version of the manuscript. For access to original osteological material used in the present study, we are grateful to the Authority for Research and Conservation of Cultural Heritage (ARCCH), Ethiopian Ministry of Culture and Tourism and the curatorial staff of the National Museum of Addis Ababa. Funding was provided by the Actions Incitatives of the Université de Poitiers and the Conseil Général de la Vienne (ACI 2013-2014), the French National Research Agency (Project ANR ARCHOR 12-CULT-0006, dir. S. Harmand), the Omo Group Research Expedition (dir. J.-R. Boisserie). Lastly, we thank also G. Florent and G. Reynaud for their administrative guidance.

References

Alba, D.M., Moyà-Solà, S., Köhler, M., 2003. Morphological affinities of the *Australopithecus afarensis* hand on the basis of manual proportions and relative thumb length. J. Hum. Evol. 44, 225–254.

Almécija, S., Alba, D.M., 2014. On manual proportions and pad-to-pad precision grasping in *Australopithecus afarensis*. J. Hum. Evol. 73, 88–92.

Almécija, S., Moyà-Solà, S., Alba, D.M., 2010. Early origin for human-like precision grasping: A comparative study of pollical distal phalanges in fossil hominins. PLoS ONE 5, e11727, http://dx.doi.org/10.1371/journal.pone.0011727.

Almécija, S., Smaers, J.B., Jungers, W.L., 2015. The evolution of human and ape hand proportions. Nat. Commun. 6, 7717, http://dx.doi.org/10.1038/ncomms8717.

An, K.N., Chao, E.Y., Cooney 3rd., W.P., Linscheid, R.L., 1979. Normative model of human hand for biomechanical analysis. J. Biomech. 12, 775–788.

An, K.N., Ueba, Y., Chao, E.Y., Cooney, W.P., Linscheid, R.L., 1983. Tendon excursion and moment arm of index finger muscles. J. Biomech. 16, 419–425.

Batmanabane, M., Malathi, S., 1985. Movements at the carpometacarpal and metacarpophalangeal joints of the hand and their effect on the dimensions of the articular ends of the metacarpal bones. The Anat. Rec. 213, 102–110.

Boesch, C., Boesch, H., 1993. Different hand postures for pounding nuts with natural hammers by wild chimpanzees. In: Preuschoft, H., Chivers, D.J. (Eds.), Hands of Primates. Springer-Verlag, New York, pp. 91–108.

Bolsterlee, B., Vardy, A.N., van der Helm, F.C.T., Veeger (DirkJan), H.E.J., 2015. The effect of scaling physiological cross-sectional area on musculoskeletal model predictions. J. Biomech. 48, 1760–1768.

Bush, M.E., 1982. Hominid carpal, metacarpal, and phalangeal bones recovered from the Hadar Formation: 1974-1977 collections. Am. J. Phys. Anthropol. 57, 651–677.

Chao, E.Y., 1989. Biomechanics of the hand: a basic research study. World Scientific.

Chaudhari, A.J., Leahy, R.M., Wise, B.L., Lane, N.E., Badawi, R.D., Joshi, A.A., 2014. Global point signature for shape analysis of carpal bones. Phys. Med. Biol. 59, 961–973.

Daver, G., Berillon, G., Grimaud-Hervé, D., 2012. Carpal kinematics in quadrupedal monkeys: towards a better understanding of wrist morphology and function: Carpal kinematics in quadrupedal monkeys. J. Anat. 220, 42–56.

Delp, S.L., Anderson, F.C., Arnold, A.S., Loan, P., Habib, A., John, C.T., Guendelman, E., Thelen, D.G., 2007. OpenSim: Open-source software to create and analyze dynamic simulations of movement. Biomed. Eng. IEEE Trans. On 54, 1940–1950.

Diogo, R., Richmond, B.G., Wood, B., 2012. Evolution and homologies of primate and modern human hand and forearm muscles, with notes on thumb movements and tool use. J. Hum. Evol. 63, 64–78.

Domalain, M.F., Seitz, W.H., Evans, P.J., Li, Z.-M., 2011. Biomechanical effect of increasing or decreasing degrees of freedom for surgery of trapeziometacarpal joint arthritis: A simulation study. J. Orthop. Res. 29, 1675–1681.

Domalain, M.F., Vigouroux, L., Berton, E., 2010. Determination of passive moment-angle relationships at the trapeziometacarpal joint. J. Biomech. Eng. 132, 071009–71017.

Domínguez-Rodrigo, M., Pickering, T.R., Bunn, H.T., 2010. Configurational approach to identifying the earliest hominin butchers. Proc. Natl. Acad. Sci. U. S. A. 107, 20929–20934.

Drapeau, M.S.M., 2015. Metacarpal torsion in apes, humans, and early *Australopithecus*: implications for manipulatory abilities. Peer J. 3, e1311, http://dx.doi.org/10.7717/peerj.1311.

Drapeau, M.S.M., Ward, C.V., 2007. Forelimb segment length proportions in extant hominoids and *Australopithecus afarensis*. Am. J. Phys. Anthropol. 132, 327–343.

Drapeau, M.S.M., Ward, C.V., Kimbel, W.H., Johanson, D.C., Rak, Y., 2005. Associated cranial and forelimb remains attributed to *Australopithecus afarensis* from Hadar, Ethiopia. J. Hum. Evol. 48, 593–642.

Dubosset, J.F., 1981. Finger rotation during prehension. In: Tubiana, R. (Ed.), The Hand. W.B. Saunders Company, Philadelphia, pp. 202–206.

El-Shennawy, M., 2001. Three-dimensional kinematic analysis of the second through fifth carpometacarpal joints. J. Hand. Surg. 26, 1030–1035.

Gabra, J.N., Li, Z.-M., 2016. Three-dimensional stiffness of the carpal arch. J. Biomech. 49, 53–59.

Goislard de Monsabert, B., Rossi, J., Berton, E., Vigouroux, L., 2012. Quantification of hand and forearm muscle forces during a maximal power grip task. Med. Sci. Sports Exerc. 44, 1906–1916.

Goislard de Monsabert, B., Vigouroux, L., Bendahan, D., Berton, E., 2014. Quantification of finger joint loadings using musculoskeletal modelling clarifies mechanical risk factors of hand osteoarthritis. Med. Eng. Phys. 36, 177–184.

Harmand, S., Lewis, J.E., Feibel, C.S., Lepre, C.J., Prat, S., Lenoble, A., Boës, X., Quinn, R.L., Brenet, M., Arroyo, A., Taylor, N., Clément, S., Daver, G., Brugal, J.-P., Leakey, L., Mortlock, R.A., Wright, J.D., Lokorodi, S., Kirwa, C., Kent, D.V., Roche, H., 2015. 3.3-million-year-old stone tools from Lomekwi 3, West Turkana, Kenya. Nature 521, 310–315.

Hicks, J.L., Uchida, T.K., Seth, A., Rajagopal, A., Delp, S.L., 2015. Is my model good enough? Best practices for verification and validation of musculoskeletal models and simulations of movement. J. Biomech. Eng. 137, 020905, http://dx.doi.org/10.1115/1.4029304.

Hollister, A., Buford, W.L., Myers, L.M., Giurintano, D.J., Novick, A., 1992. The axes of rotation of the thumb carpometacarpal joint. J. Orthop. Res. 10, 454–460.

Holzbaur, K.R.S., Murray, W.M., Delp, S.L., 2005. A model of the upper extremity for simulating musculoskeletal surgery and analyzing neuromuscular control. Ann. Biomed. Eng. 33, 829–840.

Hutchinson, J.R., 2004. Biomechanical modeling and sensitivity analysis of bipedal running ability. II. Extinct taxa. J. Morphol. 262, 441–461.

Isler, K., 2006. Inertial properties of hominoid limb segments. J. Anat. 209, 201–218.

Jacobson, M.D., Raab, R., Fazeli, B.M., Abrams, R.A., Botte, M.J., Lieber, R.L., 1992. Architectural design of the human intrinsic hand muscles. J. Hand Surg. 17, 804–809.

Johanson, D.C., Taieb, M., Coppens, Y., 1982. Pliocene hominids from the Hadar Formation. Ethiopia (1973-1977): stratigraphic, chronologic, and paleoenvironmental contexts, with notes on hominid morphology and systematics. Am. J. Phys. Anthropol. 57, 373–402.

Key, A.J.M., Dunmore, C.J., 2015. The evolution of the hominin thumb and the influence exerted by the non-dominant hand during stone tool production. J. Hum. Evol. 78, 60–69.

Kivell, T.L., Kibii, J.M., Churchill, S.E., Schmid, P., Berger, L.R., 2011. *Australopithecus sediba* hand demonstrates mosaic evolution of locomotor and manipulative abilities. Science 333, 1411–1417.

Lee, J.H., Asakawa, D.S., Dennerlein, J.T., Jindrich, D.L., 2015. Finger muscle attachments for an OpenSim Upper-Extremity Model. PLoS ONE 10, e0121712, http://dx.doi.org/10.1371/journal.pone.0121712.

Latimer, B., 1991. Locomotor adaptations in *Australopithecus afarensis*: the issue of arboreality. In: Coppens, Y., Senut, B. (Eds.), Origine(s) de la Bipédie chez les Hominidés. CNRS, Paris, pp. 169–176.

Li, Z.-M., Tang, J., 2007. Coordination of thumb joints during opposition. J. Biomech. 40, 502–510.

Li, Z.-M., Zatsiorsky, V.M., Latash, M.L., 2001. The effect of finger extensor mechanism on the flexor force during isometric tasks. J. Biomech. 34, 1097–1102.

Lieber, R., Jacobson, M., Fazeli, B., Abrams, R., Botte, M., 1992. Architecture of selected muscles of the arm and forearm: anatomy and implications for tendon transfer. J. Hand Surg. Am. 17, 799–804.

Majors, B.J., Wayne, J.S., 2011. Development and validation of a computational model for investigation of wrist biomechanics. Ann. Biomed. Eng. 39, 2807–2815.

Marzke, M.W., 1983. Joint functions and grips of the *Australopithecus afarensis* hand, with special reference to the region of the capitate. J. Hum. Evol. 12, 197–211.

Marzke, M.W., 1997. Precision grips, hand morphology, and tools. Am. J. Phys. Anthropol. 102, 91–110.

Marzke, M.W., 2013. Tool making, hand morphology and fossil hominins. Phil. Trans. R. Soc. B Biol. Sci. 368, 20120414, http://dx.doi.org/10.1098/rstb.2012.0414.

Marzke, M.W., Shackley, M.S., 1986. Hominid hand use in the Pliocene and Pleistocene: Evidence from experimental archaeology and comparative morphology. J. Hum. Evol. 15, 439–460.

Marzke, M.W., Wullstein, K.L., 1996. Chimpanzee and human grips: A new classification with a focus on evolutionary morphology. Int. J. Primatol. 17, 117–139.

Marzke, M.W., Toth, N., Schick, K., Reece, S., Steinberg, B., Hunt, K., Linscheid, R.L., An, K., 1998. EMG study of hand muscle recruitment during hard hammer percussion manufacture of Oldowan tools. Am. J. Phys. Anthropol. 105, 315–332.

McFadden, D., Bracht, M.S., 2005. Sex differences in the relative lengths of metacarpals and metatarsals in gorillas and chimpanzees. Horm. Behav. 47, 99–111.

McPherron, S.P., Alemseged, Z., Marean, C.W., Wynn, J.G., Reed, D., Geraads, D., Bobe, R., Bearat, H.A., 2010. Evidence for stone-tool-assisted consumption of animal tissues before 3.39 million years ago at Dikika, Ethiopia. Nature 466, 857–860.

Mirakhorlo, M., Visser, J.M.A., Goislard de Monsabert, B.A.A.X., van der Helm, F.C.T., Maas, H., Veeger, H.E.J., 2016. Anatomical parameters for musculoskeletal modeling of the hand and wrist. Int. Biomech. 3, 40–49.

Nagano, A., Umberger, B.R., Marzke, M.W., Gerritsen, K.G.M., 2005. Neuromusculoskeletal computer modeling and simulation of upright, straight-legged, bipedal locomotion of *Australopithecus afarensis* (A.L 288-1). Am. J. Phys. Anthropol. 126, 2–13.

Nicolas, G., Multon, F., Berillon, G., 2009. From bone to plausible bipedal locomotion, Part II: Complete motion synthesis for bipedal primates. J. Biomech. 42, 1127–1133.

Ogihara, N., Kunai, T., Nakatsukasa, M., 2005. Muscle dimensions in the chimpanzee hand. Primates J. Primatol. 46, 275–280.

Orr, C.M., Leventhal, E.L., Chivers, S.F., Marzke, M.W., Wolfe, S.W., Crisco, J.J., 2010. Studying primate carpal kinematics in three dimensions using a computed-tomography-based markerless registration method. Anat. Rec. Adv. Integr. Anat. Evol. Biol. 293, 692–709.

Prilutsky, B.I., Zatsiorsky, V.M., 2002. Optimization-based models of muscle coordination. Exerc. Sport. Sci. Rev. 30, 32.

Ricklan, D.E., 1987. Functional anatomy of the hand of *Australopithecus africanus*. J. Hum. Evol. 16, 643–664.

Rolian, C., Gordon, A.D., 2013. Reassessing manual proportions in *Australopithecus afarensis*. Am. J. Phys. Anthropol. 152, 393–406.

Rolian, C., Lieberman, D.E., Hallgrímsson, B., 2010. The coevolution of human hands and feet. Evolution 64, 1558–1568.

Rolian, C., Lieberman, D.E., Zermeno, J.P., 2011. Hand biomechanics during simulated stone tool use. J. Hum. Evol. 61, 26–41.

Romero, F., Alonso, F.J., 2016. A comparison among different Hill-type contraction dynamics formulations for muscle force estimation. Mech. Sci. 7, 19–29.

Rossi, J., Goislard de Monsabert, B., Berton, E., Vigouroux, L., 2015. Handle shape affects the grip force distribution and the muscle loadings during power grip tasks. J. Appl. Biomech. 31, 430–438.

Sancho-Bru, J.L., Perez-Gonzalez, A., Vergara, M., Giurintano, D.J., 2003. A 3D biomechanical model of the hand for power grip. J. Biomech. Eng. 125, 78–83.

Skinner, M.M., Stephens, N.B., Tsegai, Z.J., Foote, A.C., Nguyen, N.H., Gross, T., Pahr, D.H., Hublin, J.-J., Kivell, T.L., 2015. Human-like hand use in *Australopithecus africanus*. Science 347, 395–399.

Stern Jr., J.T., Susman, R.L., 1983. The locomotor anatomy of *Australopithecus afarensis*. Am. J. Phys. Anthropol. 60, 279–317.

Susman, R.L., 1998. Hand function and tool behavior in early hominids. J. Hum. Evol. 35, 23–46.

Thompson, J.C., McPherron, S.P., Bobe, R., Reed, D., Barr, W.A., Wynn, J.G., Marean, C.W., Geraads, D., Alemseged, Z., 2015. Taphonomy of fossils from the hominin-bearing deposits at Dikika, Ethiopia. J. Hum. Evol. 86, 112–135.

Tocheri, M.W., Marzke, M.W., Liu, D., Bae, M., Jones, G.P., Williams, R.C., Razdan, A., 2003. Functional capabilities of modern and fossil hominid hands: Three-dimensional analysis of trapezia. Am. J. Phys. Anthropol. 122, 101–112.

Tuttle, R.H., 1969. Quantitative and functional studies on the hands of the Anthropoidea, I. The Hominoidea. J. Morph. 128, 309–363.

Valero-Cuevas, F.J., Johanson, M.E., Towles, J.D., 2003. Towards a realistic biomechanical model of the thumb: the choice of kinematic description may be more critical than the solution method or the variability/uncertainty of musculoskeletal parameters. J. Biomech. 36, 1019–1030.

Vigouroux, L., Domalain, M., Berton, E., 2009. Comparison of tendon tensions estimated from two biomechanical models of the thumb. J. Biomech. 42, 1772–1777.

Vigouroux, L., Domalain, M., Berton, E., 2011. Effect of object width on muscle and joint forces during thumb-index finger grasping. J. Appl. Biomech. 27, 176–180.

Villmoare, B., Kimbel, W.H., Seyoum, C., Campisano, C.J., DiMaggio, E.N., Rowan, J., Braun, D.R., Arrowsmith, J.R., Reed, K.E., 2015. Early *Homo* at 2.8 Ma from Ledi-Geraru, Afar, Ethiopia. Science 347, 1352–1355.

Wang, W., Crompton, R.H., Carey, T.S., Günther, M.M., Li, Y., Savage, R., Sellers, W.I., 2004. Comparison of inverse-dynamics musculo-skeletal models of AL 288-1 *Australopithecus afarensis* and KNM-WT 15000 *Homo ergaster* to modern humans, with implications for the evolution of bipedalism. J. Hum. Evol. 47, 453–478.

Ward, C.V., Kimbel, W.H., Harmon, E.H., Johanson, D.C., 2012. New postcranial fossils of *Australopithecus afarensis*from Hadar, Ethiopia (1990-2007). J. Hum. Evol. 63, 1–51.

Williams, E.M., Gordon, A.D., Richmond, B.G., 2010. Upper limb kinematics and the role of the wrist during stone tool production. Am. J. Phys. Anthropol. 143, 134–145.

Williams, E.M., Gordon, A.D., Richmond, B.G., 2012. Hand pressure distribution during Oldowan stone tool production. J. Hum. Evol. 62, 520–532.

Williams, E.M., Gordon, A.D., Richmond, B.G., 2014. Biomechanical strategies for accuracy and force generation during stone tool production. J. Hum. Evol. 72, 52–63.